Quantum Electronics **48** (5) 448–452 (2018)

https://doi.org/10.1070/QEL16664

Doppler laser cooling and vibrational spectrum of $^{24}Mg^+$ ions in a linear Paul trap

I.V. Zalivako, A.S. Borisenko, I.A. Semerikov, K.Yu. Khabarova, N.N. Kolachevsky

Abstract. **We report results on the laser cooling of $^{24}Mg^+$ ions to temperatures below 80 mK in a linear quadrupole Paul trap. A method has been demonstrated for determining secular frequencies of ions using amplitude modulation of cooling light, and vibrational spectra of simple ion crystals have been investigated.**

Keywords: *laser cooling, Paul ion trap, spectroscopy, dynamics of ions.*

1. Introduction

Owing to the simple design and reliability of ion traps and the good isolation of ions from external disturbances, spatially localised and deeply cooled ions are excellent subjects of research aimed at resolving a variety of basic and applied issues. For example, Penning traps are used for antihydrogen synthesis [1] and precision measurements of the fine structure constant [2]. RF Paul traps are employed to study new optical frequency standards [3] and realise quantum logic elements [4], are planned for use in deep cooling of antihydrogen [5], etc. At present, research effort is concentrated on optical frequency standards based on strontium [6], aluminium [7], ytterbium [8] and other metal ions. In particular, an optical clock based on a single ytterbium ion in a three-dimensional Paul trap and designed at the National Metrology Institute of Germany (PTB) offers a relative uncertainty of 3×10^{-18} [8], which has made it possible to place stringent limitations on the drift of the fine structure constant.

In addition to optical standards, localised ions are widely used to address quantum logic issues and realise quantum computing elements. In such a case, quantum information is recorded and stored in the internal state of ions, and logical operations are performed by coupling the ions through their vibrational degrees of freedom in the trap potential [9]. The ion qubits are then completely identical and demonstrate record long coherence times (up to 10 min) [10] and a small gate error (no greater than 4×10^{-5} for single-qubit operations [11] and less than 10^{-3} for two-qubit CNOT gates [11]), which sets them apart from superconducting and neutral-atom qubits [12]. At present, researchers address scale-up issues [13] and the transition to ion traps on chips [14].

Methods developed for constructing single-ion quantum logic elements found application as well in the spectroscopy of optical frequency standards. In particular, a sympathetic cooling method was proposed, which enables ions that have no suitable cooling transition to be cooled to low temperatures. Cooling is here due to Coulomb interaction with an additional refrigerant ion, which can be laser-cooled directly [15]. In addition to the sympathetic cooling of the spectroscopy ion, the auxiliary ion makes it possible to detect its state using quantum logic [16]. These methods allowed one to considerably extend the range of ions that can be cooled to their vibrational ground state in the trap potentional. For the implementation of the quantum logic method in precision spectroscopy – the creation of high-accuracy $^{27}Al^+$ optical clocks with $^{25}Mg^+$ as a logic ion – D.J. Wineland was awarded the 2012 Nobel Prize in Physics (shared with S. Haroche).

Our group is conducting research into the laser cooling of $^{25}Mg^+$ ions with the aim of creating efficient quantum interfaces. The $^{25}Mg^+$ ion has a nonzero nuclear spin, which leads to hyperfine splitting of its levels. A transition between hyperfine components of the ground state of an ion is often used as a microwave qubit. The advantages of this ion for application in quantum logic include its simple energy level structure and the availability of laser sources for experiments with it. Moreover, just one laser system is sufficient for dealing with this ion [17]. In a number of laboratories in the world, researchers demonstrated successful laser cooling of magnesium ions to the Doppler limit and vibrational ground state [3, 17, 18]. A preparatory stage in our research was $^{24}Mg^+$ and $^{26}Mg^+$ trapping and laser cooling experiments. These isotopes have no hyperfine splitting, so they cannot be used for quantum logic studies, but they are significantly easier to deal with owing to their simpler level structure.

The key objectives in the first stage of our work were the laser cooling of ions, the implementation of ion crystal detection methods and investigation of the vibrational degrees of freedom of simple ion strings. The results obtained are important for further experimental studies of $^{25}Mg^+$ cooling to its vibrational ground state and for research into the entanglement of states of several ions via their common vibrational modes. From their vibrational spectrum, one can determine the mass of ions of other trapped isotopes or elements. A special role is then played by axial vibrational modes, because typically it is such modes that are responsible for the interaction between particles in an ion trap.

I.V. Zalivako, A.S. Borisenko, I.A. Semerikov, K.Yu. Khabarova
P.N. Lebedev Physical Institute, Russian Academy of Sciences, Leninsky prosp. 53, 119991 Moscow, Russia;
e-mail: zalikes@yandex.ru;
N.N. Kolachevsky P.N. Lebedev Physical Institute, Russian Academy of Sciences, Leninsky prosp. 53, 119991 Moscow, Russia; Russian Quantum Center, Novaya ul. 100, Skolkovo, 143025 Moscow, Russia

Received 21 February 2018; revision received 12 March 2018
Kvantovaya Elektronika **48** (5) 448–452 (2018)
Translated by O.M. Tsarev

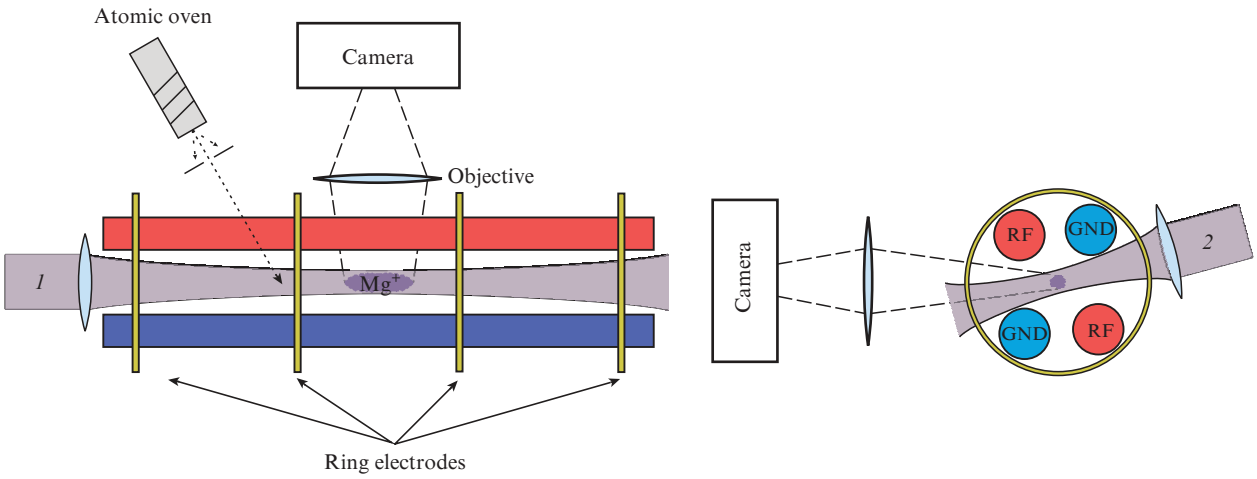

Figure 1. (Colour online) Schematic of the experimental setup for $^{24}Mg^+$ confinement and cooling (top view in the left panel and side view in the right panel): (*1*, *2*) laser beams that ensure cooling (beam *1* is parallel to the trap axis, and beam *2* makes an angle with all three trap axes); RF and GND are electrodes for radial ion confinement.

2. Experimental setup

Figure 1 shows a schematic of the experimental setup. In our experiments, ions are confined using a linear Paul trap which was described in detail elsewhere [19]. Radial confinement in it is ensured by four cylindrical electrodes, two of which are earthed. To the other two electrodes, an ac voltage is applied, with a frequency $\omega = 2\pi\times 18$ MHz and amplitude V_{ac} that can be varied from zero to 600 V. Axial ion confinement is ensured by four ring electrodes located along the trap axis. A dc voltage $V_{ax} = 500$ V is applied to them.

The trap is situated in a vacuum chamber, which is maintained at a pressure below 10^{-10} Torr by a getter-ion pump. Light reaches the ions in the trap through antireflection-coated quartz windows of the vacuum chamber. Magnesium ions are loaded into the trap using an atomic oven consisting of a magnesium-filled metallic tube and electric heater. When the tube is heated, the magnesium vaporises and, after passing through two diaphragms, forms a narrow atomic beam, which passes through the trapping region. The atoms in the beam are ionised by electron impact in the confinement region of the trap.

The four ring electrodes that ensure axial confinement divide the trap into three sections, each capable of trapping ions. The trapped ions can be transferred from one section to another by varying the voltage applied to the electrodes. The presence of several sections allows one to load and precool ions in one part of the trap and measure spectra and manipulate quantum states in another. Separating the working and loading regions of the trap significantly reduces the effect the parasitic electric fields resulting from magnesium ionisation. The atomic beam passes through one of the lateral sections, where the particles become trapped, following which the ions are transferred to the central section.

Around the radial confinement electrodes, there are another four cylindrical electrodes, to which dc voltages can be applied to compensate for the parasitic electric fields in the particle localisation region. The parasitic electric field shifts the equilibrium position of the ions from the trap axis, leading to heating of the particles and undesirable shifts of spectral lines [20].

The magnesium ions are cooled on the $^2S_{1/2} \rightarrow {}^2P_{3/2}$ strong cyclic transition by radiation with a wavelength $\lambda = 280$ nm. The natural linewidth Γ of this transition is $2\pi\times 41$ MHz. Figure 2 shows a schematic of the laser system for magnesium ion cooling. It is built around a Toptica TA Pro semiconductor laser emitting at a wavelength of 1120 nm. The laser is equipped with a tapered amplifier, and its output power is 830 mW. Next, two home-built second-harmonic generators based on LBO and BBO nonlinear crystals [21] ensure two-stage conversion of 1120-nm radiation to the fourth harmonic, with a wavelength of 280 nm. The 280-nm radiation is used for ion cooling. The UV power at the output of the final second-harmonic generator is 10 mW. The laser wavelength is stabilised using an Angstrom WS-U wavemeter (at the fundamental frequency), which ensures frequency stability in an about 1-MHz band.

To ensure the possibility of rapidly changing the cooling light frequency and intensity, the optical scheme includes a double-pass acousto-optic modulator (AOM). After the AOM, the light is divided into two beams (*1*, *2*), one of which enters the trap along its axis and the other enters the trap at

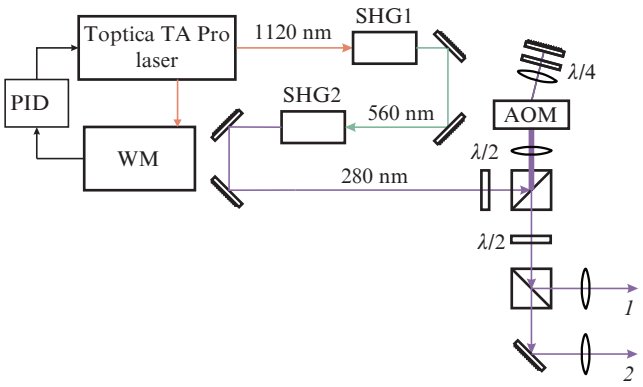

Figure 2. Schematic of the laser system for magnesium ion cooling: (PID) PID controller; (WM) WS-U wavemeter; (SHG1, SHG2) 1120 → 560 and 560 → 280 nm frequency doubling stages, respectively; (AOM) acousto-optic modulator; (*1*, *2*) laser beams.

an angle to its three axes. The former beam makes it possible to significantly improve cooling efficiency in the trapping stage, because it covers most of the trapping region, and the latter ensures efficient cooling of all the degrees of freedom of the particles after transfer of the trapped particles to the working section.

The fluorescence of the trapped ions is collected by a large-aperture $5^{\times}$ objective consisting of quartz lenses with a 280-nm antireflection coating. This radiation is detected by a photomultiplier or highly sensitive EMCCD camera, depending on experimental parameters.

3. Laser cooling of $^{24}Mg^{+}$ ions

The first step in our ion cooling experiments was ion trapping. The cooling laser, detuned from the frequency of the transition by 2Γ to the red, operated throughout this step, and the atomic oven and ionisation source were turned on. Depending on the atomic oven current and loading time, not only single particles but also large ion crystals and clouds can be trapped (Fig. 3). After the loading, the ions were transferred to the working section of the trap by changing the voltage applied to the ring electrodes. Concurrently, the detuning of the cooling light was reduced to 1Γ. Since electron impact ionisation is not selective, the trap often contained, in addition to $^{24}Mg^{+}$ ions, ions of other magnesium isotopes and components of the residual gas in the vacuum chamber, which could be represented in an image by blank spaces in the periodic structure of ion crystals ('dark' ions). If the number of 'dark' ions is sufficiently large, heating of such ions may prevent ion cloud crystallisation. To remove 'dark' ions from the trap, it was cleaned after loading. To this end, the radial confinement field of the trap was switched off at intervals for a time of the order of a few microseconds, during which ions noninteracting with light left the trapping region because they had higher kinetic energy. A few seconds of such cleaning are ususally sufficient for crystallisation of the ions. A longer procedure makes it possible to obtain pure crystals, consisting only of fluorescing particles of the desired magnesium isotope.

After the ion loading, we compensated the parasitic electric fields. To this end, the amplitude of the ac confinement field of the trap was reduced and a voltage was applied to the compensating electrodes such that ion images on the camera did not shift.

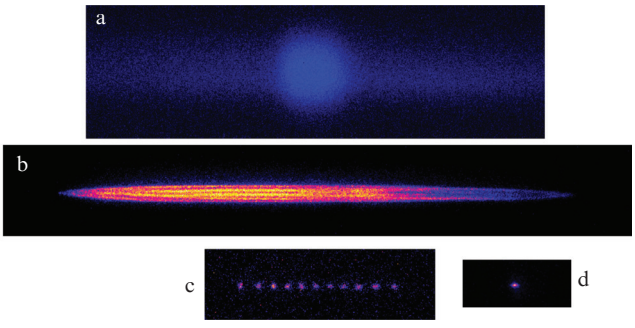

Figure 3. (Colour online) Images of different types of ion clouds and crystals obtained at different cooling parameters and loading times: (a) noncrystalline cloud of $^{24}Mg^{+}$ ions; (b) ion crystal consisting of 10^3 to 10^4 particles; (c) string of 11 ions; (d) single ion.

To estimate the temperature reached by the ions during laser cooling, we measured the single-ion fluorescence intensity as a function of cooling light detuning (Fig. 4). The ion fluorescence was detected by an EMCCD camera. The light intensity at the ion localisation point corresponded to saturation intensity. In accordance with Doppler cooling theory, the ion temperature began to rise sharply near the resonance frequency, which led to ion delocalisation and, in the case of a transition through resonance to the blue region, escape of the ion from the trap because of the strong heating by light. In Fig. 4, ion delocalisation shows up as a sharp decrease in fluorescence signal.

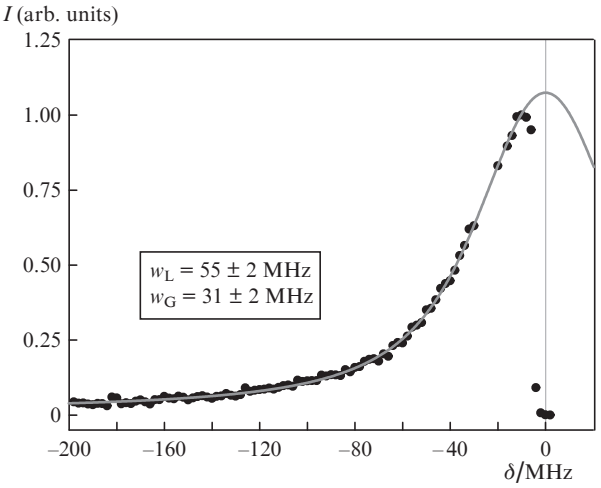

Figure 4. Variation in the fluorescence intensity of a single ion as the cooling light frequency detuning is scanned from the red to the blue spectral region. The sharp drop in intensity near the resonance corresponds to heating-induced ion delocalisation. The solid line represents the best fit to the data with a Voigt function.

The data in Fig. 4 are well fitted by a Voigt function. The width of its Lorentzian component is $w_L = 55 \pm 2$ MHz and that of its Gaussian component is $w_G = 31 \pm 2$ MHz. The width of the Lorentzian component roughly corresponds to the power-broadened magnesium $^2S_{1/2} \rightarrow {}^2P_{3/2}$ linewidth. The Gaussian component is due to the first-order Doppler effect and is associated with the fact that, at the axial frequencies admissible in our trap, the Lamb–Dicke regime cannot be reached by Doppler cooling. The obtained width of the Gaussian component corresponds to Doppler broadening at a temperature $T =$ 40 mK. It is important to note however that the temperature obtained in this way is a rough estimate because scanning the frequency is accompanied by changes in cooling parameters and, hence, in temperature. Thus, scanning the frequency leads to changes in the Doppler broadening of the line. Given the large number of experiments at various cooling parameters and taking into account that the temperature estimated by the method in question is the upper estimate, it is reasonable to conclude that, in our experiments, the ion temperature was below 80 mK – or even below 40 mK at optimised parameters.

Our experiments on the trapping and Doppler cooling of $^{26}Mg^{+}$ ions indicate that the results obtained for $^{26}Mg^{+}$ ions are similar to those for $^{24}Mg^{+}$ ions.

4. Secular spectrum of simple ion crystals

To study vibrational frequencies in the potential of the trap, the laser light amplitude was modulated using AOM. The vibrational frequency of ions was measured by scanning the modulation frequency of beams *1* and *2* (Fig. 1). At the instant when the modulation frequency coincides with the vibrational frequency of an ion, the vibration amplitude, observed using a camera, rises. Figure 5 shows images of an ion in the cases when the modulation frequency is far from secular eigenfrequencies of a single ion (Fig. 5a, far from resonance), coincides with the axial frequency of ion motion (Fig. 5b) and coincides with the radial frequency of ion motion (Fig. 5c). The axial and radial resonances are a few kilohertz in width.

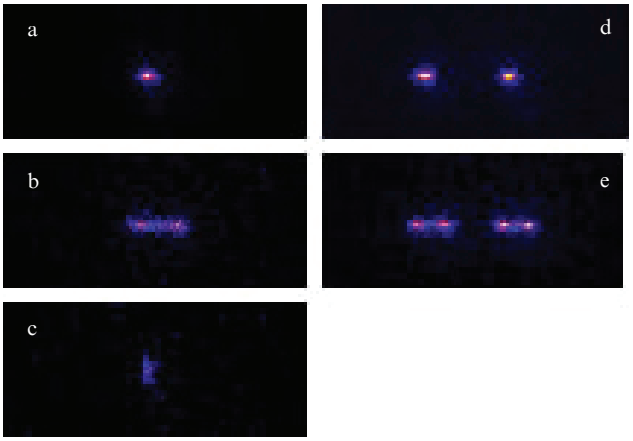

Figure 5. (Colour online) Images of elementary $^{24}Mg^+$ crystals, obtained with a camera by scanning secular frequencies. The left panels are images of a single ion at different modulation frequencies: (a) the modulation frequency of the cooling light is far from resonance; (b) the modulation frequency coincides with the axial vibration frequency; (c) the modulation frequency coincides with the radial vibration frequency. The right panels are images of a pair of ions at the instants when the modulation frequency (d) differs from their vibrational eigenmodes and (e) coincides with the axial vibration frequency.

The axial vibration frequency depends on the voltage applied to the inner ring electrodes, V_{ax}. In the case of a single $^{24}Mg^+$ ion at V_{ax} = 500 V, the axial frequency is $\Omega_{ax} = 2\pi\times(51.5\pm1.0)$ kHz.

Radial vibration frequencies depend on both the voltage applied to the ring electrodes, V_{ax}, and the amplitude of the voltage applied to the cylindrical electrodes of the trap, V_{ac}. According to theory, the radial frequency should be a linear function of the RF confinement field amplitude at a constant voltage applied to the inner electrodes [22]. Figure 6 shows the measured radial frequency ω_{rad} as a function of V_{ac} at V_{ax} = 500 V, where the vertical axis shows a voltage proportional to V_{ac}, which was measured using a voltage divider. Comparison of these data with theory allows the divider to be accurately calibrated, which offers the possibility of controlling the secular frequencies of ions and the trap depth with high accuracy.

In addition, we measured axial vibration frequencies of a crystal consisting of two $^{24}Mg^+$ ions (Figs 5d, 5e). According to theory, a crystal consisting of two ions should have two vibrational eigenfrequencies: inphase, $\Omega_{ax}^{i} = \Omega_{ax}$, and antiphase, $\Omega_{ax}^{o} = \sqrt{3}\,\Omega_{ax}$, where Ω_{ax} is the axial vibration frequency of a single ion. The measured frequencies are $\Omega_{ax}^{i} = 2\pi\times(51.5\pm1.0)$ kHz and $\Omega_{ax}^{o} = 2\pi\times(91.0\pm1.0)$ kHz, which supports the above theoretical estimates.

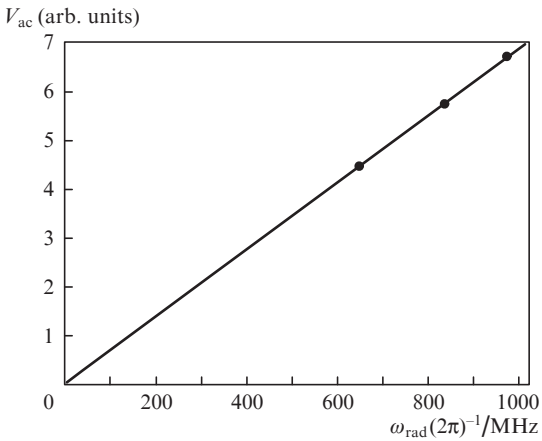

Figure 6. Radial secular frequency as a function of RF confinement field amplitude for a single $^{24}Mg^+$ ion in the trap. The solid line represents the best fit straight line.

The described experiments aimed at determining vibrational eigenfrequencies of single ions and small ion crystals are important for planned experiments on the cooling of $^{25}Mg^+$ ions to their vibrational ground state [3] and the entanglement of states of several ions via their common vibrational modes. The linear relationship in Fig. 6 points to high harmonicity of the trap pseudopotential in the axial direction, which in turn ensures a slow heating rate and the possibility of deep cooling of ions.

5. Conclusions

We have presented our results on the Doppler cooling of $^{24}Mg^+$ and $^{26}Mg^+$ ions in a linear Paul trap designed for experimental studies of quantum interfaces and implementation of the quantum logic method. According to a conservative estimate, the ion temperature at the end of the Doppler cooling step is under 80 mK. We have investigated the secular frequency spectrum of simple ion crystals: a single $^{24}Mg^+$ ion and a $^{24}Mg^+$ ion pair. The results demonstrate that, in radial direction, the pseudopotential of the Paul trap possesses high harmonicity, which ensures a slow microwave heating rate and opens up the possibility of deep cooling of $^{25}Mg^+$ions to their vibrational ground state. In a crystal consisting of two ions, we have excited inphase and antiphase vibrational modes with frequencies $\Omega_{ax}^{i} = 2\pi\times(51.5\pm1.0)$ kHz and $\Omega_{ax}^{o} = 2\pi\times(91.0\pm1.0)$ kHz. We have demonstrated the possibility of targeted excitation of a particular mode, which is an important step to the implementation of the quantum logic method for ion pair and CNOT gate realisation.

Acknowledgements. This work was supported by the Russian Science Foundation (Grant No. 16-12-00096).

References

1. Amoretti M., Amsler C., Bonomi G., Bouchta A., Bowe P., Carraro C., Cesar C.L., Chaliton M., Collier M.J.T., Doser M., Filippini V., Fine F.S., Fontana A., Fujiwara M.C., Funakoshi R., Genova P., Hangst J.S., Hayano R.S., Holzscheiter M.H., Jørgensen L.V., Lagomarsino V., Landua R., Lindelöf D., Rizzini E.L., Macrì M., Madsen N., Manuzio G., Marchesotti M., Montagna P., Pruys H.,

Regenfus C., Riedler P., Rochet J., Rotondi A., Rouleau G., Testera G., Variola A., Watson T.L., Van Der Werf D.P. *Nature*, **419**, 456 (2002).
2. Hanneke D., Fogwell S., Gabrielse G. *Phys. Rev. Lett*., **100**, 120801 (2008).
3. Chou C.W., Hume D.B., Koelemeij J.C.J., Wineland D.J., Rosenband T. *Phys. Rev. Lett*., **104**, 8 (2010).
4. Debnath S., Linke N.M., Figgatt C., Landsman K.A., Wright K., Monroe C. *Nature*, **536**, 63 (2016).
5. Pérez P., Banerjee D., Biraben F., Brook-Roberge D., Charlton M., Cladé P., Comini P., Crivelli P., Dalkarov O., Debu P., Douillet A., Dufour G., Dupré P., Eriksson S., Froelich P., Grandemange P., Guellati S., Guérout R., Heinrich J.M., Hervieux P.A., Hilico L., Husson A., Indelicato P., Jonsell S., Karr J.P., Khabarova K., Kolachevsky N., Kuroda N., Lambrecht A., Leite A.M.M., Liszkay L., Lunney D., Madsen N., Manfredi G., Mansoulié B., Matsuda Y., Mohri A., Mortensen T., Nagashima Y., Nesvizhevsky V., Nez F., Regenfus C., Rey J.M., Reymond J.M., Reynaud S., Rubbia A., Sacquin Y., Schmidt-Kaler F., Sillitoe N., Staszczak M., Szabo-Foster C.I., Torii H., Vallage B., Valdes M., Van der Werf D.P., Voronin A., Walz J., Wolf S., Wronka S., Yamazaki Y. *Hyperfine Interact*., **233**, 21 (2015).
6. Barwood G.P., Huang G., King S.A., Klein H.A., Gill P. *J. Phys. B, At. Mol. Opt. Phys*., **48**, 035401 (2015).
7. Rosenband T., Hume D.B., Schmidt P.O., Chou C.W., Brusch A., Lorini L., Oskay W.H., Drullinger R.E., Fortier T.M., Stalnaker J.E., Diddams S.A., Swann W.C., Newbury N.R., Itano W.M., Wineland D.J., Bergquist J.C. *Science*, **319**, 1808 (2008).
8. Huntemann N., Sanner C., Lipphardt B., Tamm C., Peik E. *Phys. Rev. Lett*., **116**, 63001 (2016).
9. Schmidt-Kaler F., Häffner H., Riebe M., Gulde S., Lancaster G.P.T., Deutschle T., Becher C., Roos C.F., Eschner J., Blatt R. *Nature*, **422**, 408 (2003).
10. Wang Y., Um M., Zhang J., An S., Lyu M., Zhang J.N., Duan L.M., Yum D., Kim K. *Nat. Photonics*, **11**, 646 (2017).
11. Gaebler J.P., Tan T.R., Lin Y., Wan Y., Bowler R., Keith A.C., Glancy S., Coakley K., Knill E., Leibfried D., Wineland D.J. *Phys. Rev. Lett*., **117**, 1 (2016).
12. Saffman M. *J. Phys. B At. Mol. Opt. Phys*., **49**, 202001 (2016).
13. Zhang J., Pagano G., Hess P.W., Kyprianidis A., Becker P., Kaplan H., Gorshkov A.V., Gong Z.-X., Monroe C. *Nature*, **551**, 601 (2017).
14. Brandl M.F., Van Mourik M.W., Postler L., Nolf A., Lakhmanskiy K., Paiva R.R., Möller S., Daniilidis N., Häffner H., Kaushal V., Ruster T., Warschburger C., Kaufmann H., Poschinger U.G., Schmidt-Kaler F., Schindler P., Monz T., Blatt R. *Rev. Sci. Instrum*., **87**, 113103 (2016).
15. Barrett M.D., DeMarco B., Schaetz T., Meyer V., Leibfried D., Britton J., Chiaverini J., Itano W.M., Jelenković B., Jost J.D., Langer C., Rosenband T., Wineland D.J. *Phys. Rev. A*, **68**, 42302 (2003).
16. Schmidt P.O., Rosenband T., Langer C., Itano W.M., Bergquist J.C., Wineland D.J. *Science*, **309**, 749 (2005).
17. Hemmerling B., Gebert F., Wan Y., Nigg D., Sherstov I.V., Schmidt P.O. *Appl. Phys. B*, **104**, 583 (2011).
18. Batteiger V., Knünz S., Herrmann M., Saathoff G., Schüssler H.A., Bernhardt B., Wilken T., Holzwarth R., Hänsch T.W., Udem T. *Phys. Rev. A, At. Mol. Opt. Phys*., **80**, 1 (2009).
19. Semerikov I.A., Zalivako I.V., Shpakovskii T.V., Borisenko A.S., Khabarova K.Yu., Kolachevsky N.N. *Quantum Electron*., **46**, 935 (2016) [*Kvantovaya Elektron*., **46**, 935 (2016)].
20. Berkeland D.J., Miller J.D., Bergquist J.C., Itano W.M., Wineland D.J. *J. Appl. Phys*., **83**, 5025 (1998).
21. Shpakovsky T.V., Zalivako I.V., Semerikov I.A., Golovizin A.A., Borisenko A.S., Khabarova K.Y., Sorokin V.N., Kolachevsky N.N. *J. Russ. Laser Res*., **37**, 440 (2016).
22. Leibfried D., Blatt R., Monroe C., Wineland D. *Rev. Mod. Phys*., **75**, 281 (2003).